Nuclear Materials and Energy 43 (2025) 101944

Contents lists available at ScienceDirect

Nuclear Materials and Energy

journal homepage: www.elsevier.com/locate/nme

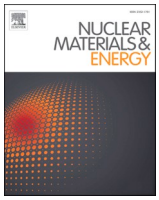

Influence of thermal treatment at various temperatures on structure and radiation-induced effects in advanced ceramic breeder pebbles

A. Ansone [a], A. Antuzevics [b], L. Avotina [a], E. Sprugis [b], A. Trimdale-Deksne [c], J.M. Leys [d], R. Knitter [d], A. Zarins [a,e,*]

[a] University of Latvia, Faculty of Science and Technology, Institute of Chemical Physics, 1 Jelgavas Str., LV-1004 Riga, Latvia
[b] Institute of Solid State Physics, University of Latvia, 8 Kengaraga Str., LV-1063 Riga, Latvia
[c] University of Latvia, Faculty of Medicine and Life Sciences, Department of Chemistry, 1 Jelgavas Str., LV-1004 Riga, Latvia
[d] Karlsruhe Institute of Technology, Institute for Applied Materials, 76021 Karlsruhe, Germany
[e] Daugavpils University, Faculty of Natural Sciences and Healthcare, Department of Environment and Technologies, 1A Parades Str., LV-5401 Daugavpils, Latvia

ARTICLE INFO

Keywords:
Advanced ceramic breeder pebbles
Tritium breeding
Thermal treatment
Crystal structure
Intrinsic and extrinsic defects
X-ray irradiation
Paramagnetic centres

ABSTRACT

Advanced ceramic breeder (ACB) pebbles consisting of 65 mol% lithium orthosilicate (Li_4SiO_4) and 35 mol% lithium metatitanate (Li_2TiO_3) are currently being developed as the European Union's reference material for tritium breeding in future thermonuclear fusion reactors. In the present work, the influence of thermal treatment at various temperatures on structure and radiation-induced effects in the ACB pebbles is investigated. The produced ACB pebbles were thermally treated at selected temperatures between 500 and 1000 °C in different atmospheres (air, argon, and vacuum) and afterwards irradiated using X-rays with energies up to 45 keV. The formed and accumulated paramagnetic radiation-induced defect centres in the irradiated ACB pebbles before and after thermal treatment were analysed using electron paramagnetic resonance (EPR) spectroscopy. To determine the exact temperatures of the phase transitions and evaluate the influence of thermal treatment on the crystal structure, chemical bond vibrations, and microstructure of the ACB pebbles before irradiation, several other relevant physico-chemical analytical methods were applied: differential scanning calorimetry/thermogravimetry (DSC/TG), powder X-ray diffraction (PXRD) technique, attenuated total reflectance – Fourier transform infrared (ATR-FTIR) spectroscopy, and scanning electron microscopy (SEM). On the basis of the obtained results, it can be concluded that thermal treatment at temperatures higher than 700 °C influences the distribution of paramagnetic centres generated by exposure to X-rays. This is probably due to the second-order phase transition from "low-temperature" to "high-temperature" structure of the Li_4SiO_4 phase between 600 and 750 °C. The obtained results highlight the importance of considering the thermal treatment temperature of the produced ACB pebbles prior to irradiation when analysing these ceramic materials using EPR spectroscopy techniques.

1. Introduction

Lithium orthosilicate (Li_4SiO_4) pebbles with additions of lithium metatitanate (Li_2TiO_3) as the second phase, also referred to as the advanced ceramic breeder (ACB) material, are currently being developed for tritium breeding in the European Union's (EU) helium cooled pebble bed (HCPB) concept design for test blanket modules (TBM) in the international thermonuclear experimental reactor (ITER) and later on for application in the demonstration thermonuclear fusion power plant (DEMO) [1–3]. Previously, both Li_4SiO_4 and Li_2TiO_3 in the form of ceramic pebbles with a diameter of about 1 mm have been extensively characterised and tested worldwide as two of the most promising solid-state lithium-containing candidate materials for tritium breeding [4]. Li_4SiO_4 pebbles have a higher lithium density and slightly better tritium release behaviour at lower temperatures, while Li_2TiO_3 pebbles have superior mechanical properties and a higher melting temperature [5]. ACB pebbles consisting of 65 mol% Li_4SiO_4 and 35 mol% Li_2TiO_3 represent the EU reference material for tritium breeding with the aim to combine the advantageous properties of both ceramic materials [3] and to meet all requirements for application in a thermonuclear fusion reactor [6]. In addition to their principal function of tritium breeding and release, the biphasic ACB pebbles must withstand the anticipated

* Corresponding author.
E-mail address: arturs.zarins@lu.lv (A. Zarins).

https://doi.org/10.1016/j.nme.2025.101944
Received 25 February 2025; Received in revised form 16 April 2025; Accepted 24 April 2025
Available online 25 April 2025

harsh operational conditions, including high neutron and other ionising radiation flux, elevated temperatures, etc. [2,7]. It is well known that the interaction mechanism and penetration depth of ionising radiation (i.e., neutrons, charged particles, and photons) in matter depends on the mass, electric charge, and energy of the incident particles [8–11]. The formation and accumulation of radiation-induced point defects (simple centres), their aggregates (complex centres), radiolysis products, and nuclear transmutation products during irradiation using high-energy neutrons can induce changes of thermal and mechanical properties, cause swelling and degradation of mechanical integrity of the ceramic pebbles [12], and consequently affect the generated tritium release behaviour [13]. Prolonged exposure to elevated temperatures can also induce the recombination of accumulated radiation-induced defect centres and radiolysis products, lead to a release of various gaseous radiolysis and nuclear transmutation products, as well as cause crystalline phase transformations and microstructural changes (e.g., grain growth, grain boundary blurring, crack initiation and propagation, volume expansion, etc.) [14–16]. Therefore, it is necessary to investigate and describe all radiation-induced effects and thermal processes in the ACB pebbles, which may occur under the simultaneous action of various ionising radiation types and elevated temperatures.

Previously, the radiation stability of the ACB pebbles, which were produced using the melt-based process of the KALOS (**KA**rlsruhe **L**ithium **O**rtho**S**ilicate) facility, before and after long-term thermal treatment has been analysed and described by Heuser et al. [17]. The produced ACB pebbles with different nominal compositions were thermally treated for up to 128 days at one selected temperature – 900 °C, which is expected to be close to the maximum temperature in the EU HCPB blanket concept for DEMO [18]. Before thermal treatment, the ACB pebbles have a dendritic microstructure of two crystalline phases: monoclinic Li_4SiO_4 and cubic Li_2TiO_3, which is metastable at room temperature and remains due to the fast-cooling rate of the melt droplets by liquid nitrogen during the KALOS process [3]. After thermal treatment, significant changes in the chemical compositions, microstructures, porosities, and mechanical properties of the ACB pebbles have not been observed, except for the transition of cubic Li_2TiO_3 into monoclinic form, which is the stable crystal structure at room temperature. After irradiation using 5 MeV accelerated electrons at room temperature, the formation and accumulation of similar radiation-induced defect centres with paramagnetic properties (containing unpaired electrons) have been detected in the ACB pebbles before and after thermal treatment [17]. During irradiation using accelerated electrons, the formation of paramagnetic centres is induced by direct ionisation, excitation mechanism (radiolysis), and single atomic displacements [19]. According to previous studies [20,21], it is expected that various paramagnetic centres are mainly forming in the Li_4SiO_4 phase of the ACB pebbles during irradiation, while the Li_2TiO_3 phase exhibits a higher radiation stability. Therefore, it is important to consider the second-order phase transition from "low-temperature" to "high-temperature" structure of the Li_4SiO_4 phase that occurs between 600 and 750 °C, which has been detected and described for various Li_4SiO_4-based ceramic materials by several authors [22–31]. During heating at temperatures higher than 1100 °C, the eutectic melting of the Li_4SiO_4 phase and the reversible transition of monoclinic Li_2TiO_3 into cubic form will occur [32], while complete melting of the ACB pebbles is expected below the melting point of pure Li_2TiO_3 at 1533 °C [33].

In the present work, the influence of thermal treatment at various temperatures on structure and radiation-induced effects in the ACB pebbles is investigated. Electron paramagnetic resonance (EPR) spectroscopy is one of the most frequently used analytical and non-destructive techniques, which has previously been specifically applied to characterise paramagnetic centres in the ACB pebbles after irradiation using various ionising radiation types [34]. Regardless of the ionising radiation type, similar EPR signals of electronic spin $S = 1/2$ systems with distinctive symmetries (i.e., isotropic, nearly axial, and rhombic), g-factor (g) values, and thermal properties have been separated and described. In the present work for the irradiation of the ACB pebbles before and after thermal treatment, the exposure to X-rays with energies up to 45 keV is selected due to the feasibility of performing the EPR spectra measurements immediately after irradiation, which allows the detection of unstable paramagnetic centres. Moreover, the crystal structure of the ACB pebbles will not be affected due to the relatively small absorbed dose. It is expected that during irradiation using X-rays, the mobile charge carriers (electrons and holes) created by the indirect ionisation will be trapped both in intrinsic defects (crystal lattice imperfections) and in extrinsic defects (impurity atoms) of the crystal structure forming paramagnetic centres. In order to complement the obtained results of EPR spectroscopy, several other relevant physico-chemical analytical methods are applied to determine the exact temperatures of the phase transitions and evaluate the influence of thermal treatment on the crystal structure, chemical bond vibrations, and microstructure of the ACB pebbles before irradiation, which is necessary to predict the possible local structure of intrinsic and extrinsic defects in the Li_4SiO_4 phase: differential scanning calorimetry/thermogravimetry (DSC/TG), powder X-ray diffraction (PXRD) technique, attenuated total reflectance – Fourier transform infrared (ATR-FTIR) spectroscopy, and scanning electron microscopy (SEM).

2. Experimental

ACB pebbles with a nominal composition of 65 mol% Li_4SiO_4 and 35 mol% Li_2TiO_3 were produced using the melt-based process of the KALOS facility [3]. The optical microscopy (OM) image of the produced ACB pebbles with a size distribution of 250–1250 μm is shown in Fig. 1. Using the determined content of silicon and titanium by inductively coupled plasma – optical emission spectrometry (ICP-OES, iCAP 7600 – ThermoFisher-Scientific), the actual composition of the ACB pebbles is evaluated to be 65.3 mol% Li_4SiO_4 and 34.7 mol% Li_2TiO_3. In order to avoid the formation and accumulation of chemisorption products, e.g., lithium hydroxide (LiOH), lithium carbonate (Li_2CO_3), lithium metasilicate (Li_2SiO_3), etc., on the surface of the ACB pebbles due to reactions of the Li_4SiO_4 phase with water (H_2O) vapour and carbon dioxide (CO_2) from air [35], the pebbles were stored in a desiccator cabinet at room temperature (about 20–25 °C) with nitrogen atmosphere and afterwards

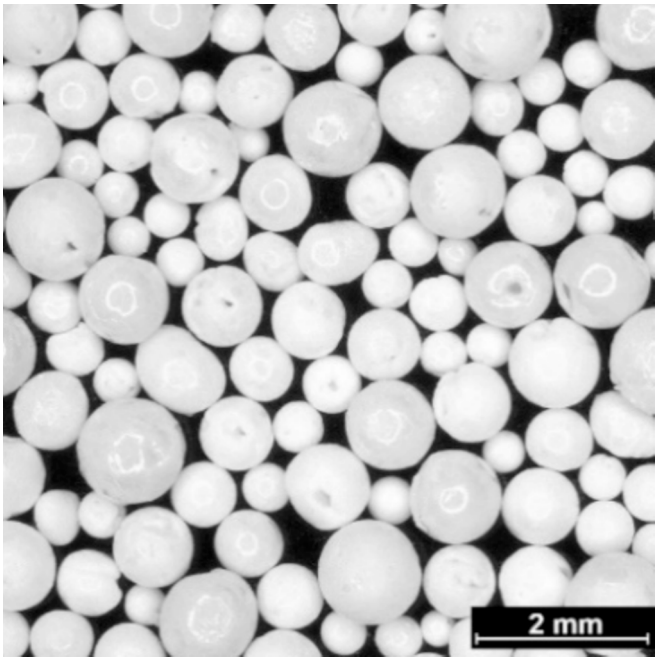

Fig. 1. OM image of the produced ACB pebbles with a size distribution of 250–1250 μm using the melt-based process of the KALOS facility.

transferred into plastic bottles and sealed into vacuumed plastic bags for transportation.

To determine the exact temperatures of the polymorphic phase transitions and the eutectic melting of the Li_4SiO_4 phase and the Li_2TiO_3 phase in the ACB pebbles, DSC/TG measurements were performed using a SETARAM – LABSYS Evo equipment. The ACB pebbles (approximately 50 mg) were transferred into an alumina (Al_2O_3) ceramic crucible (diameter: 5 mm; height: 8 mm) and afterwards heated from room temperature up to 1400 °C (5 min hold at the maximum temperature) with a heating rate of about 10 °C/min in argon atmosphere (flow rate: about 30 mL/min). The obtained DSC and TG curves were corrected by performing an automatic blank curve subtraction.

On the basis of the obtained DSC/TG results, six temperatures with an incremental step of 100 °C were selected for the thermal treatment of the ACB pebbles near or higher than the second-order phase transition temperatures of the Li_4SiO_4 phase between 600 and 750 °C, but lower than the eutectic melting temperature at about 1100 °C. The ACB pebbles (approximately 0.2 g) were transferred into an Al_2O_3 ceramic boat (width: 15 mm; length: 40 mm; height: 10 mm) and afterwards thermally treated up to 500, 600, 700, 800, 900 and 1000 °C for 1 h in different atmospheres (air, argon, and vacuum) using a custom-built thermal treatment system, which consists of a Nabertherm horizontal split-type tube furnace RSH 50/500/13, ceramic tube (diameter: 5 cm; length: 85 cm), gas supply system with vacuum-tight stainless steel water-cooled flanges, HYFRA air-type water recooler LWK 21-S, Lybold digital vacuum meter Thermovac RM101, Lybold SEGEVAC single-stage oil-sealed rotary vane pump, and charge control for the temperature measurements in the ceramic tube during thermal treatment. The temperature during thermal treatment was increased from room temperature up to 1000 °C with a heating rate of about 5 °C/min. After each thermal treatment step, the ACB pebbles were slowly cooled down to room temperature for further characterisation and irradiation experiments. The weight changes of the ACB pebbles before and after each thermal treatment step were monitored using analytic balance Precisa XR 205 SM-DR. Prior to the characterisation and irradiation experiments, the ACB pebbles before and after thermal treatment were stored in plastic bottles using a desiccator cabinet at room temperature in air with low relative humidity (about 10 RH%) at all times.

For the PXRD and ATR-FTIR measurements, the ACB pebbles before and after thermal treatment were carefully crushed into fine powders using an agate mortar at room temperature in air. The PXRD patterns were recorded from 10 up to 70° 2-theta range with a scan speed of 0.2 s / 0.02° 2-theta at room temperature in air using a Bruker D8 Discover diffractometer equipped with a CuKα source (wavelength: 0.15418 nm). The X-ray tube voltage and current were set to 40 kV and 40 mA, respectively. The ATR-FTIR spectra were measured in the range of 400–4000 cm^{-1} with a resolution of 2 cm^{-1} at room temperature in vacuum using a Bruker Vertex 70v spectrometer equipped with a diamond crystal. Each ATR-FTIR spectrum is the average of 60 sample scans (20 scans per measurement, at least 3 measurements per sample).

The SEM images for the polished and water-etched cross-sections of the ACB pebbles before and after thermal treatment, which were previously embedded into epoxy resin, were obtained using SEM SUPRA 55, Zeiss. In order to prevent the sample from charging, the prepared cross-section surface of the ACB pebbles was sputtered with gold–palladium (Au-Pd) coating using a Leica EM ACE 600 vacuum sputter coater. The thickness of the obtained coating was 4 nm, coating speed: 0.03 nm/s, temperature: 22 °C.

The ACB pebbles before and after thermal treatment were irradiated using an X-ray source operated for 30 min at room temperature in air, 45 kV voltage, and 10 mA current with an evaluated absorbed dose of about 1 kGy. EPR spectroscopy investigations were carried out with a Bruker Elexsys-II E500 spectrometer. The EPR spectra were acquired at room temperature using 9.83 GHz frequency microwave radiation with power in the 1–100 mW range, 100 kHz magnetic field modulation frequency, and 0.4 mT modulation amplitude. The EPR signal intensities have been normalised to the used mass of the ACB pebbles for each measurement.

3. Results and discussion

The obtained DSC and TG curves of the untreated ACB pebbles are shown in Fig. 2. The DSC curve displays two main groups of endothermic peaks during heating up to 1400 °C. The first group consists of two easily distinguishable peaks with maxima at about 640 and 710 °C. Both peaks are attributed to the second-order phase transition from “low-temperature” to “high-temperature” structure of the Li_4SiO_4 phase, while the previously described third peak at lower temperatures is probably below the detection limit of this method [22–31]. At temperatures higher than 1150 °C, peaks of the second group are highly overlapped. The narrow and intensive peak with a maximum at about 1200 °C can be attributed to the eutectic melting of the Li_4SiO_4 phase. However, it also needs to be considered that the reversible polymorphic transition of the Li_2TiO_3 phase (monoclinic ↔ cubic) may occur at about 1150 °C [32]. The broad peak with a maximum at about 1300 °C can probably be related to the eutectic melting of the Li_2TiO_3 phase. The TG curve indicates that weight changes of the ACB pebbles during heating are negligible. The detected weight decrease of about 0.8 wt% up to 1000 °C can be attributed to the sequential desorption of absorbed and chemisorbed H_2O vapour and CO_2, which can accumulate in minor amounts on the surface of the ACB pebbles from air during handling (including preparation, storage, and transportation) [36]. According to Cruz et al. [15], the thermal decomposition of Li_4SiO_4 by evaporation of lithium oxide and consequently the formation of Li_2SiO_3 starts between 900 and 1000 °C. As a result, the decomposition of the Li_4SiO_4 phase in the ACB pebbles during heating at temperatures higher than 900 °C cannot be completely excluded. Minor fluctuations in the TG curve above 1150 °C correlate with the eutectic melting of the Li_4SiO_4 phase and could be related to the decomposition processes in the liquid state.

Therefore, to induce the two detected endothermic processes between 600 and 750 °C, without initiating eutectic melting of the Li_4SiO_4 phase starting at about 1150 °C (Fig. 2), the untreated ACB pebbles were thermally treated at selected temperatures between 500 and 1000 °C for 1 h in air (about 1010 mbar pressure), argon (about 600 mbar at room temperature), and vacuum (about 2 mbar at room temperature). The detected weight decreases of the ACB pebbles after thermal treatment are below 1 wt%, which correlates well with the above-described results of the DSC/TG measurements. The obtained PXRD patterns of the ACB pebbles before and after thermal treatment at 1000 °C in different atmospheres and at selected temperatures in vacuum are shown in Fig. 3.

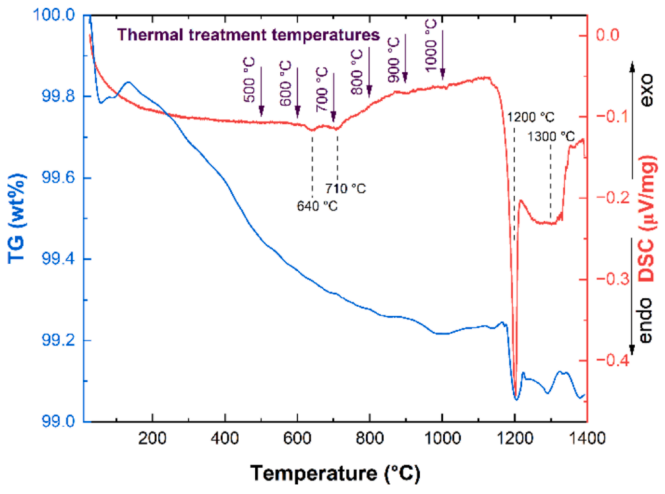

Fig. 2. DSC and TG curves of the untreated ACB pebbles with the selected temperatures for thermal treatment.

As expected from previous studies [3], the PXRD pattern of the untreated ACB pebbles contains only the characteristic reflections of monoclinic Li_4SiO_4 and cubic Li_2TiO_3. After thermal treatment regardless of the chosen atmosphere, the reflections of monoclinic Li_4SiO_4 do not change significantly, while cubic Li_2TiO_3 is gradually transformed into its monoclinic form (see left panel of Fig. 3). The obtained results also indicate that the polymorphic transition of the Li_2TiO_3 phase (cubic → monoclinic) was observed in the PXRD patterns with temperatures higher than 700 °C (see right panel of Fig. 3). Reflections related to other crystalline phases (including to the chemisorption products of H_2O vapour and CO_2, e.g., LiOH, Li_2CO_3, Li_2SiO_3, etc.) were not observed for the ACB pebbles before and after thermal treatment.

The obtained ATR-FTIR spectra of the ACB pebbles before and after thermal treatment at selected temperatures in vacuum are shown in Fig. 4. The vibrational bands with wavenumbers higher than 1800 cm^{-1} were not observed; therefore, the main focus is targeted on the bands occurring between 400 and 1800 cm^{-1} (see left panel of Fig. 4). The detected intensive bands with wavenumbers 400–1100 cm^{-1} are mainly related to the Li_4SiO_4 phase, which corresponds to a tetrahedral silicate anion (SiO_4^{4-}) structure surrounded by different lithium cations (Li^+), which occupy the interstitial space [10,36–38]. The bands below 600 cm^{-1} can be attributed to Li-O bond vibrations in LiO_n polyhedrons (n = 4,5,6), while the bands with maxima at about 800, 820, 880, 900, 920 and 950 cm^{-1} can be related to stretching and bending vibrations of Si-O bonds in SiO_4 tetrahedra. The characteristic Ti-O bond vibrations with a maximum at about 650 cm^{-1} for the Li_2TiO_3 phase [39,40] are most likely overlapping with intensive bands of the Li_4SiO_4 phase. A small intensity band with a maximum at about 1455 cm^{-1} is characteristic for Li_2CO_3 (i.e., one of the chemisorption products of CO_2) [41]. During thermal treatment at temperatures higher than 700 °C, minor changes in the ATR-FTIR spectra were observed between 700 and 800 cm^{-1} (see right panel of Fig. 4), which could be related both to intensity changes for the Ti-O bond vibrations due to the polymorphic transition of the Li_2TiO_3 phase (cubic → monoclinic) and to intensity decrease for the stretching vibrations of Si-O-Si bonds with wavenumber at about 735 cm^{-1} in Li_2SiO_3 [10]. At temperature exceeding 700 °C, both Li_2CO_3 and Li_2SiO_3 on the surface of the ACB pebbles can react with each other forming Li_4SiO_4 as one of the products [42].

The obtained SEM images for cross-sections of the ACB pebbles before and after thermal treatment at selected temperatures in vacuum are shown in Fig. 5. Two characteristic microstructure types are observed for the untreated ACB pebbles due to differences in the content of the Li_4SiO_4 phase and the Li_2TiO_3 phase, which have been investigated and described in detail by Leys et al. [43] and Heuser et al. [18]. It is important to note that the Li_4SiO_4 phase is dissolved between the dendrites of the Li_2TiO_3 phase during the water-etching step in the preparation processes of the cross-section, which is why the Li_2TiO_3 dendrites dominate the images. The first microstructure type has fine Li_2TiO_3 dendrites, while the second microstructure type has large Li_2TiO_3 dendrites (light grey grains), which were distributed between the Li_4SiO_4 phase (dark grey grains). It is expected that these two microstructure types in the ACB pebbles form during the KALOS process when the two phases partly separate in the melt. Depending on the composition of the melt, different microstructures form during rapid cooling in the process. After thermal treatment, major changes in the microstructure of the ACB pebbles, including significant grain growth, were not observed, which correlates well with previous studies [18].

The obtained EPR spectra of the irradiated ACB pebbles before and after thermal treatment at 1000 °C in different atmospheres and at selected temperatures in vacuum are shown in Fig. 6. EPR spectra were measured for the ACB pebbles after irradiation using X-rays in order to characterise the influence of thermal treatment on radiation-induced effects by detecting paramagnetic centres, which can be used as probes for observing changes to intrinsic and extrinsic defects in the crystal structure of the ACB pebbles. To refer to different positions in the EPR spectra, it is informative to introduce the effective g value (g_{eff}) using the equation:

$$g_{eff} = h\nu/\mu_B B \quad (1)$$

where h – the Planck's constant, ν – experimental microwave frequency, μ_B – the Bohr magneton, and B – magnetic field.

The evolution of EPR spectra for the irradiated ACB pebbles before and after thermal treatment (Fig. 6), microwave power saturation characteristics of different EPR signals (Fig. 7), and prior studies of irradiated ceramic materials with similar compositions [10,17,20,21] enable the separation of four main components in the obtained spectra. Arrows at g_{eff} = 2.04, 2.02, and 2.00 mark three isotropic EPR signals with symmetric Gaussian profiles, corresponding to distinct paramagnetic centres in the irradiated ACB pebbles. The g_{eff} = 2.04 and 2.02 signals are attributed to trapped-hole centres, probably associated with intrinsic defects related to oxygen ions, which exhibit instability at room temperature [20]. The g_{eff} = 2.00 signal contrasts other EPR signals by

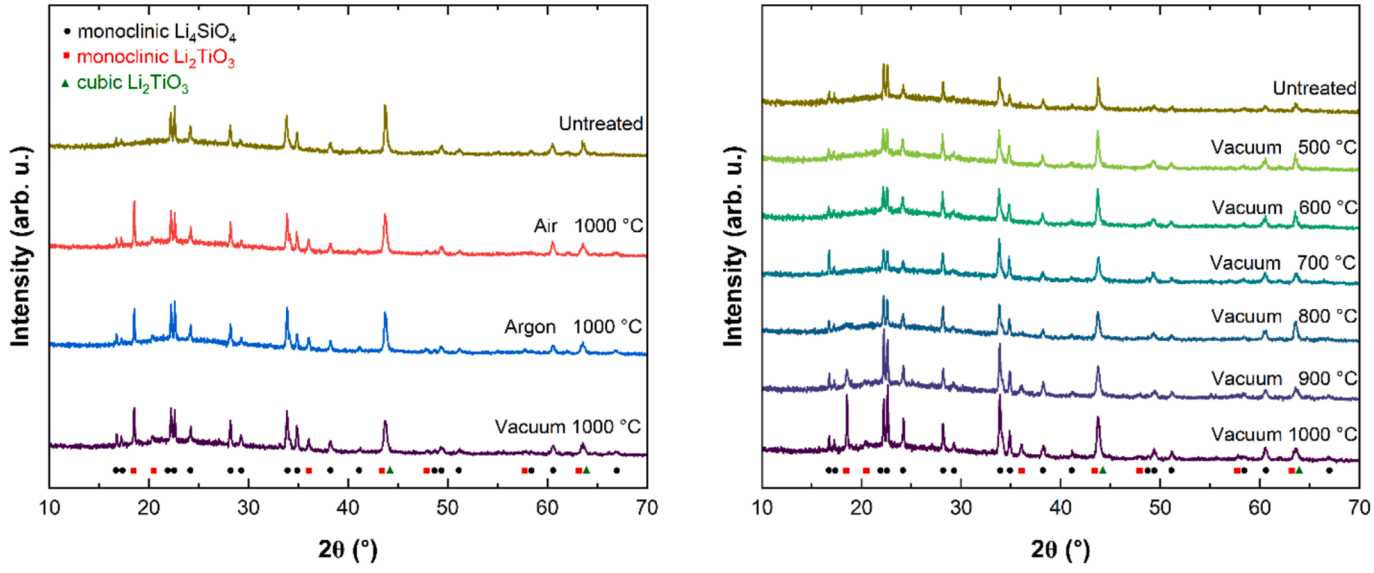

Fig. 3. PXRD patterns of the ACB pebbles before and after thermal treatment at about 1000 °C in different atmospheres (left); before and after thermal treatment at selected temperatures in vacuum (right).

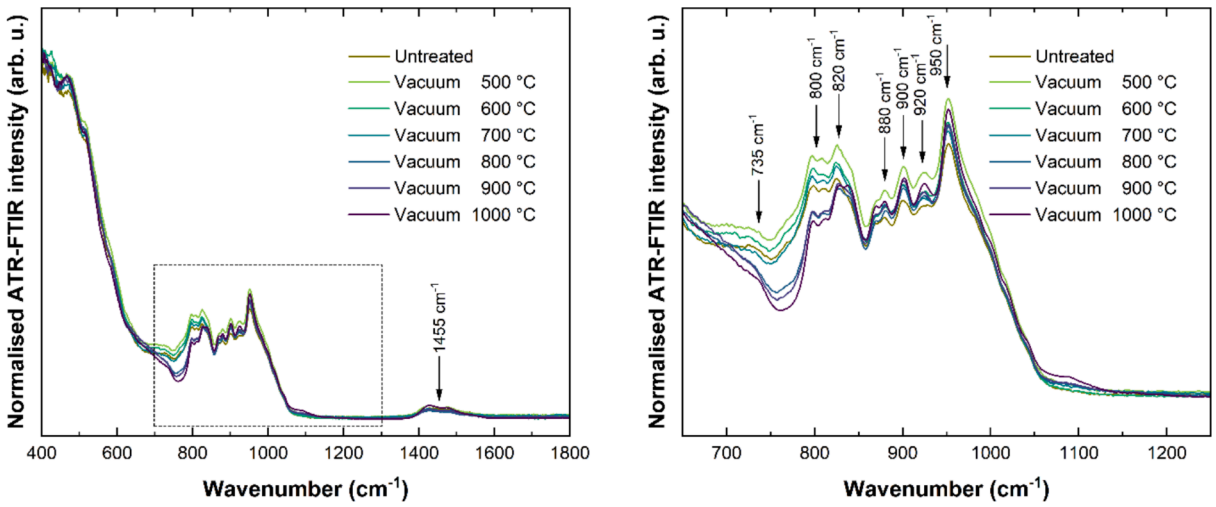

Fig. 4. Normalised ATR-FTIR spectra of the ACB pebbles before and after thermal treatment at selected temperatures in vacuum.

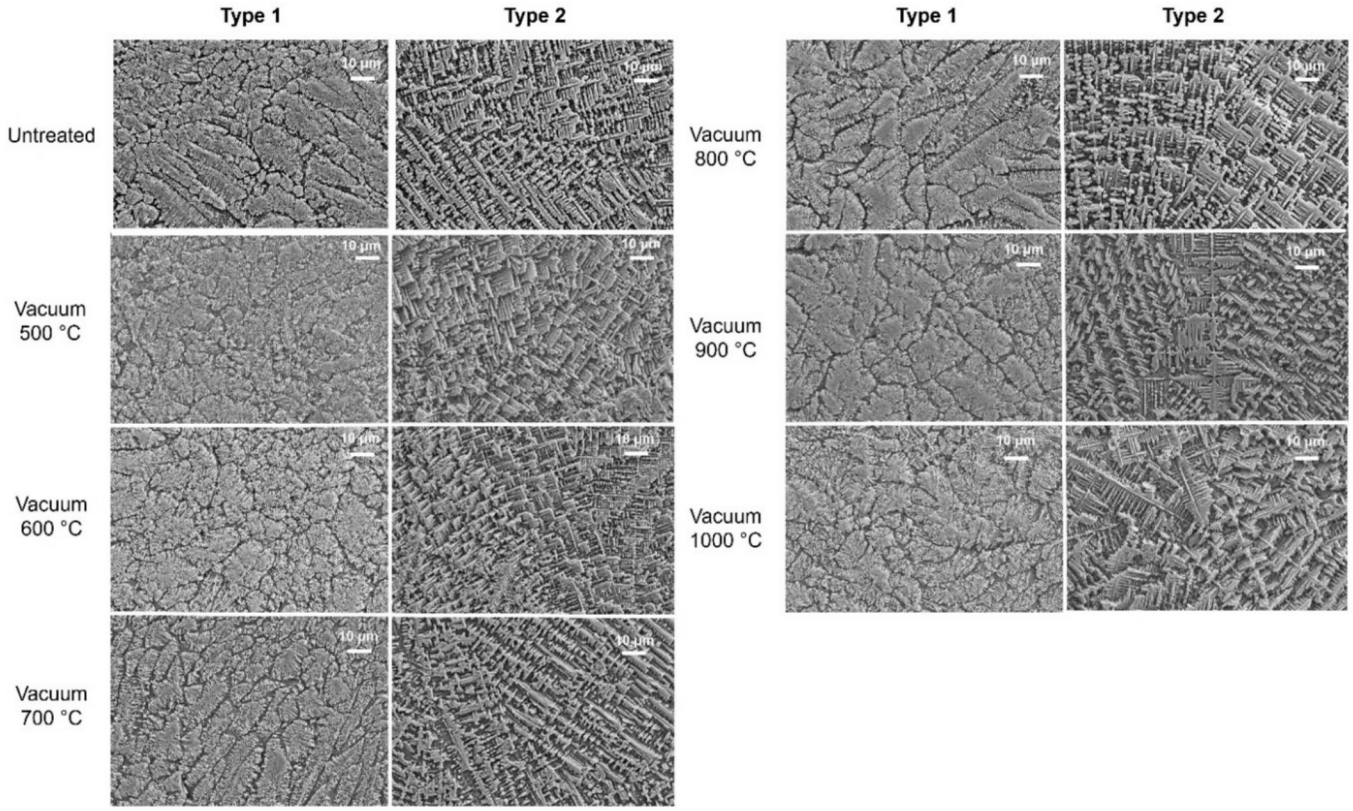

Fig. 5. SEM images of two characteristic microstructure types for cross-sections of the ACB pebbles before and after thermal treatment at selected temperatures in vacuum.

saturation at microwave power values exceeding 1 mW (Fig. 7). Although commonly ascribed to E'-type centres (in the simplest case, an unpaired electron localised on a dangling tetrahedral (sp^3) orbital of a single silicon atom) [10,11], this interpretation is ambiguous as the g value is close to the free electron value of 2.0023, and no additional features are resolved. The fourth component ($g_{eff} < 2.00$) refers to the 352–370 mT region, which contains several highly overlapped anisotropic signals (e.g., nearly axial and rhombic) with varying thermal stabilities [20]. The g values and hyperfine couplings with magnetic ^{7}Li and ^{1}H nuclei determined from previous electron nuclear double resonance (ENDOR) studies suggest that these stable EPR signals could originate from titanium-related electron centres in the Li_4SiO_4 phase of the ACB pebbles [21]. The precursor of these titanium-related electron centres could be Ti^{4+} ions (extrinsic defects) from the Li_2TiO_3 phase, which substitute silicon sites in isolated SiO_4 tetrahedra forming TiO_4 tetrahedra. After exposure to X-rays, these sites may trap electrons formed by the indirect ionisation leading to a change in the oxidation state of titanium from + 4 to + 3.

The thermal treatment of the produced ACB pebbles impacts the distribution of paramagnetic centres generated by exposure to X-rays. As depicted in the left panel of Fig. 6, a major increase of the $g_{eff} = 2.00$ signal is observed after thermal treatment at 1000 °C, while the thermal

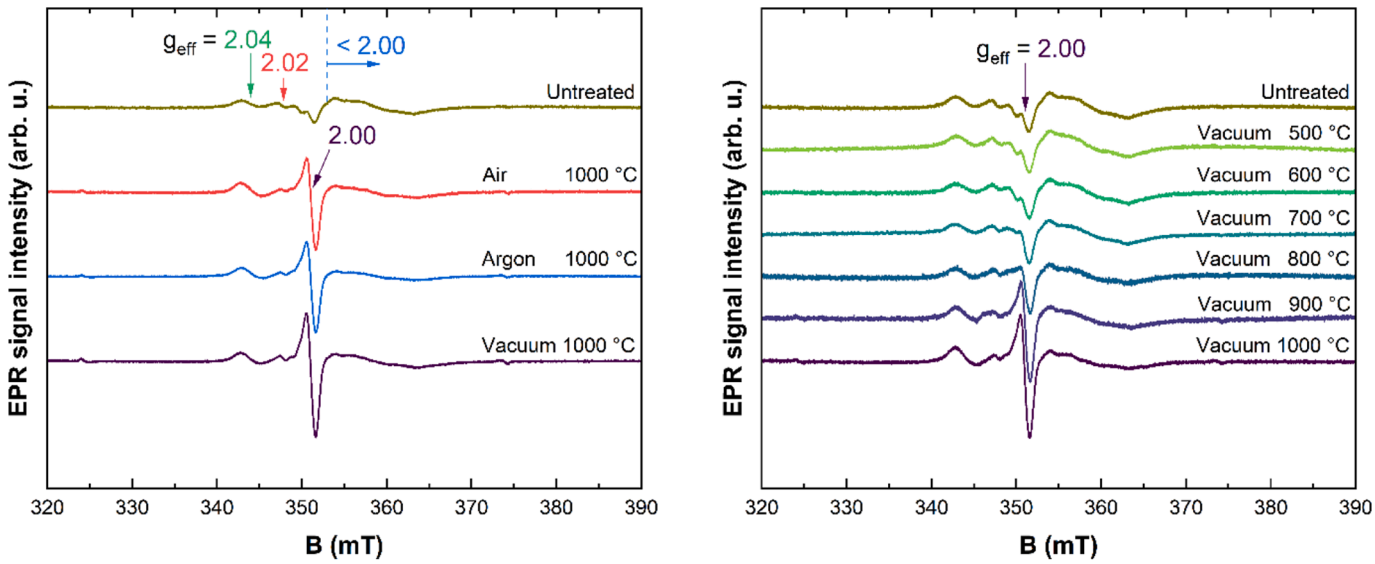

Fig. 6. EPR spectra (1 mW microwave power) of the irradiated ACB pebbles before and after thermal treatment at 1000 °C in different atmospheres (left); before and after thermal treatment at selected temperatures in vacuum (right).

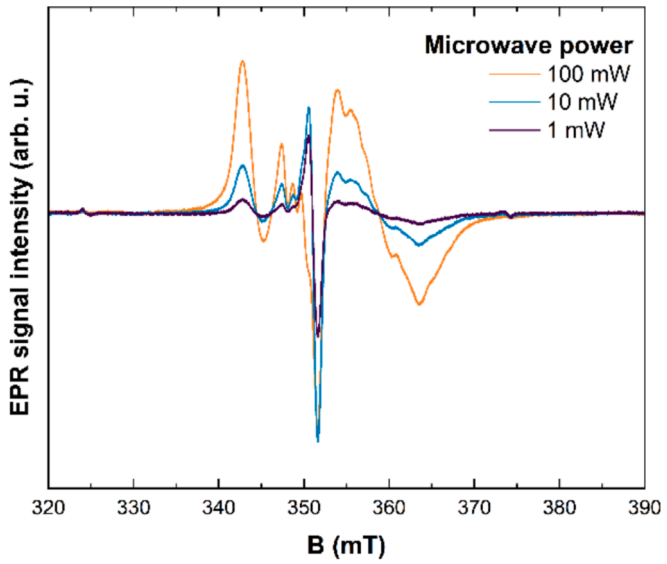

Fig. 7. EPR spectra dependence on microwave power of the irradiated ACB pebbles after thermal treatment at 1000 °C in vacuum.

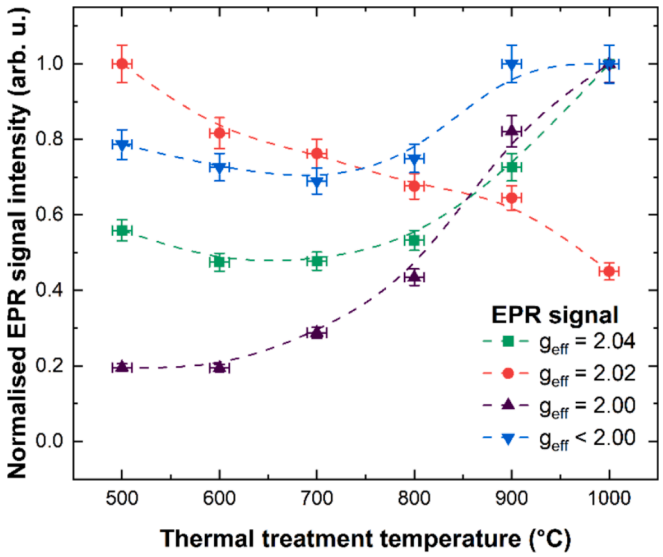

Fig. 8. Double-integrated intensities of EPR signals in the irradiated ACB pebbles as a function of selected thermal treatment temperature.

treatment atmosphere has only a relatively minor influence. The transformation process of the $g_{eff} = 2.00$ signal occurs after thermal treatment at temperatures higher than 700 °C (see right panel of Fig. 6). Analysis of the individual paramagnetic centres also reveals correlating intensity increases for the $g_{eff} = 2.04$ and $g_{eff} < 2.00$ signals (Fig. 8). In contrast, the paramagnetic centres associated with $g_{eff} = 2.02$ signal exhibits a steady decrease in intensity with thermal treatment temperature.

The obtained results indicate that the two detected endothermic processes occurring between 600 and 750 °C in the untreated ACB pebbles (Fig. 2) and the redistribution of paramagnetic centres generated by exposure to X-rays in the pebbles after thermal treatment at temperatures higher than 700 °C (Fig. 8) are partially correlated. After thermal treatment up to 1000 °C, significant changes in the crystal structure (Fig. 3), chemical bond vibrations (Fig. 4), and microstructure (Fig. 5) of the Li_4SiO_4 phase have not been observed, except for the polymorphic transition of the Li_2TiO_3 phase (cubic → monoclinic) and the sequential desorption of absorbed and chemisorbed H_2O vapour and CO_2 in minor amounts from the surface of the ACB pebbles. However, the polymorphic transition of the Li_2TiO_3 phase is not expected to have a major impact, as the observed paramagnetic centres following exposure to X-rays are associated with the Li_4SiO_4 phase of the ACB pebbles [20,21]. It can be concluded that thermal treatment at temperatures higher than 700 °C influences the intensity of individual paramagnetic centres probably due to the second-order phase transition from "low-temperature" to "high-temperature" structure of the Li_4SiO_4 phase between 600 and 750 °C. This also leads to changes in the distribution of intrinsic and extrinsic defects in the crystal structure of the ACB pebbles where electrons and holes can be trapped during irradiation. The fast-cooling rate of the melt droplets by liquid nitrogen during the KALOS process could strongly influence the distribution of charge traps in the ACB pebbles. More specifically, the rapid cooling may induce a similar effect to that observed in glasses [44,45] by "freezing" various intrinsic defects in the crystal structure of the Li_4SiO_4 phase. Subsequent thermal treatment followed by gradual cooling enables the reversible polymorphic phase transition in the Li_4SiO_4 phase, which changes the

distribution of intrinsic defects in the crystal structure. It should be emphasised that this effect is not expected to play a significant role in the long-term operation of the ACB pebbles in thermonuclear fusion reactors. However, the obtained results highlight the importance of considering the thermal treatment temperature of the produced ACB pebbles prior to irradiation when analysing these ceramic materials using EPR spectroscopy techniques.

Conclusions

The present work investigated and described the influence of thermal treatment at various temperatures on structure and radiation-induced effects in the ACB pebbles. The obtained results reveal that thermal treatment at temperatures higher than 700 °C influences the formation of individual paramagnetic radiation-induced defect centres probably due to the second-order phase transition from "low-temperature" to "high-temperature" structure of the Li_4SiO_4 phase between 600 and 750 °C. This reversible polymorphic phase transition during thermal treatment consequently changes the distribution of intrinsic and extrinsic defects in the crystal structure of the produced ACB pebbles, where created electrons and holes can be trapped during irradiation using X-rays. The most notable change in the irradiated ACB pebbles after thermal treatment is increase in the concentration of stable paramagnetic centres with a g-factor value of 2.00. No other significant changes in the crystal structure, chemical bond vibrations, and microstructure of the Li_4SiO_4 phase are observed after thermal treatment, except for the polymorphic transition of the Li_2TiO_3 phase (cubic → monoclinic) and the sequential desorption of absorbed and chemisorbed H_2O vapour and CO_2 in minor amounts from the surface of the ACB pebbles. The obtained results highlight the importance of considering the thermal treatment temperature of the produced ACB pebbles prior to irradiation when analysing these ceramic materials using EPR spectroscopy techniques.

CRediT authorship contribution statement

A. Ansone: Writing – review & editing, Writing – original draft, Methodology, Investigation, Formal analysis, Conceptualization. **A. Antuzevics:** Writing – review & editing, Writing – original draft, Visualization, Methodology, Investigation, Formal analysis, Conceptualization. **L. Avotina:** Writing – review & editing, Methodology, Investigation, Formal analysis. **E. Sprugis:** Writing – review & editing, Methodology, Investigation, Formal analysis. **A. Trimdale-Deksne:** Writing – review & editing, Methodology, Investigation, Formal analysis. **J.M. Leys:** Writing – review & editing, Resources, Methodology, Investigation, Formal analysis, Conceptualization. **R. Knitter:** Writing – review & editing, Supervision, Resources, Project administration. **A. Zarins:** Writing – review & editing, Writing – original draft, Supervision, Resources, Project administration, Methodology, Investigation, Formal analysis, Conceptualization.

Declaration of competing interest

The authors declare that they have no known competing financial interests or personal relationships that could have appeared to influence the work reported in this paper.

Acknowledgements

This work has been carried out within the framework of the EUROfusion Consortium, funded by the European Union via the Euratom Research and Training Programme (Grant Agreement No. 101052200 – EUROfusion), and the Recovery and Resilience Facility project "Internal and External Consolidation of the University of Latvia" (No. 5.2.1.1.i.0/2/24/I/CFLA/007), postdoctoral research grant No. LU-BA-PG-2024/1-0007. Views and opinions expressed are however those of the author(s) only and do not necessarily reflect those of the European Union or the European Commission. Neither the European Union nor the European Commission can be held responsible for them.

Institute of Solid State Physics, University of Latvia as the Center of Excellence has received funding from the European Union's Horizon 2020 Framework Programme H2020-WIDESPREAD-01-2016-2017-TeamingPhase2 under grant agreement No. 739508, project CAMART2.

Data availability

Data will be made available on request.

References

[1] L. Forest, L.V. Boccaccini, L. Cogneau, A.L. Puma, H. Neuberger, S. Pascal, J. Rey, N. Thomas, J. Tosi, M. Zmitko, Test blanket modules (ITER) and breeding blanket (DEMO): history of major fabrication technologies development of HCLL and HCPB and status, Fusion Eng. Des. 154 (2020) 111493, https://doi.org/10.1016/J.FUSENGDES.2020.111493.

[2] L.V. Boccaccini, F. Arbeiter, P. Arena, J. Aubert, L. Bühler, I. Cristescu, A. Del Nevo, M. Eboli, L. Forest, C. Harrington, F. Hernandez, R. Knitter, H. Neuberger, D. Rapisarda, P. Sardain, G.A. Spagnuolo, M. Utili, L. Vala, A. Venturini, P. Vladimirov, G. Zhou, Status of maturation of critical technologies and systems design: breeding blanket, Fusion Eng. Des. 179 (2022) 113116, https://doi.org/10.1016/J.FUSENGDES.2022.113116.

[3] O. Leys, J.M. Leys, R. Knitter, Current status and future perspectives of EU ceramic breeder development, Fusion Eng. Des. 164 (2021) 112171, https://doi.org/10.1016/j.fusengdes.2020.112171.

[4] R. Knitter, P. Chaudhuri, Y.J. Feng, T. Hoshino, I.-K. Yu, Recent developments of solid breeder fabrication, J. Nucl. Mater. 442 (2013) S420–S424, https://doi.org/10.1016/j.jnucmat.2013.02.060.

[5] M. Zmitko, P. Vladimirov, R. Knitter, M. Kolb, O. Leys, J. Heuser, H.-C. Schneider, R. Rolli, V. Chakin, S. Pupeschi, L. Magielsen, A. Fedorov, Y. Poitevin, Development and qualification of functional materials for the European HCPB TBM, Fusion Eng. Des. 136 (2018) 1376–1385, https://doi.org/10.1016/j.fusengdes.2018.05.014.

[6] C.E. Johnson, Ceramic breeder materials, Ceram. Int. 17 (1991) 253–258, https://doi.org/10.1016/0272-8842(91)90019-V.

[7] L. Forest, N. Thomas, L. Cogneau, J. Tosi, J. Vallory, M. Zmitko, Y. Poitevin, M. Soldaini, G.A. Spagnuolo, C. Lacroix, M. Simon-Perret, Fabrication technologies implemented for the European test blanket modules: status for HCPB and WCLL, Fusion Eng. Des. 164 (2021) 112201, https://doi.org/10.1016/J.FUSENGDES.2020.112201.

[8] T. Kulsartov, Z. Zaurbekova, R. Knitter, A. Shaimerdenov, Y. Chikhray, S. Askerbekov, A. Akhanov, I. Kenzhina, G. Kizane, Y. Kenzhin, M. Aitkulov, D. Sairanbayev, Y. Gordienko, Y. Ponkratov, Studies of two-phase lithium ceramics Li_4SiO_4-Li_2TiO_3 under conditions of neutron irradiation, Nucl. Mater. Energy 30 (2022) 101129, https://doi.org/10.1016/J.NME.2022.101129.

[9] J. Ba, R. Zeng, X. Yan, R. Li, W. Wu, F. Li, X. Xiang, D. Meng, T. Tang, Long-term helium bubble evolution in sequential He^+ and H^+ irradiated Li_4SiO_4, Ceram. Int. 47 (2021) 32310–32317, https://doi.org/10.1016/J.CERAMINT.2021.08.126.

[10] J.M. Leys, A. Zarins, J. Cipa, L. Baumane, G. Kizane, R. Knitter, Radiation-Induced effects in neutron- and electron-irradiated lithium silicate ceramic breeder pebbles, J. Nucl. Mater. 540 (2020) 152347, https://doi.org/10.1016/J.JNUCMAT.2020.152347.

[11] Q. Qi, B. Ji, S. Gu, Y. Zhang, H. Zhou, G.-N. Luo, Annihilation behavior of irradiation defects induced by γ-ray in biphasic tritium breeding materials xLi_2TiO_3-(1-x) Li_4SiO_4, Ceram. Int. 47 (2021) 434–438, https://doi.org/10.1016/j.ceramint.2020.08.150.

[12] K. Noda, T. Nakazawa, Y. Ishii, K. Fukai, H. Matsui, D. Vollath, H. Watanabe, Radiation damage in lithium orthosilicate, Mater. Trans. JIM 34 (1993) 1150–1154, https://doi.org/10.2320/matertrans1989.34.1150.

[13] Y. Zhang, Q. Zhou, A. Yang, A. Sanfukuji, Y. Oya, Tritium release behavior and application of a release model for the neutron-irradiated biphasic lithium ceramics, Fusion Eng. Des. 206 (2024) 114593, https://doi.org/10.1016/j.fusengdes.2024.114593.

[14] J.E. Tiliks, G.K. Kizane, A.A. Supe, A.A. Abramenkovs, J.J. Tiliks, V.G. Vasiljev, Formation and properties of radiation-induced defects and radiolysis products in lithium orthosilicate, Fusion Eng. Des. 17 (1991) 17–20, https://doi.org/10.1016/0920-3796(91)90029-P.

[15] D. Cruz, S. Bulbulian, E. Lima, H. Pfeiffer, Kinetic analysis of the thermal stability of lithium silicates (Li_4SiO_4 and Li_2SiO_3), J. Solid State Chem. 179 (2006) 909–916, https://doi.org/10.1016/j.jssc.2005.12.020.

[16] Y. Gong, J. Li, L. Liu, Z. Li, L. Zhuo, G. Zhang, In-situ generation of Li_2TiO_3/Li_2SiO_3 particles in Li_4SiO_4 using TiO_2 addition for grain refinement and improved thermal cycling stability, Ceram. Int. 50 (2024) 42976–42985, https://doi.org/10.1016/j.ceramint.2024.08.144.

[17] J.M. Heuser, A. Zarins, L. Baumane, G. Kizane, R. Knitter, Radiation stability of long-term annealed bi-phasic advanced ceramic breeder pebbles, Fusion Eng. Des. 138 (2019) 395–399, https://doi.org/10.1016/j.fusengdes.2018.12.034.

[18] J.M. Heuser, M.H.H. Kolb, T. Bergfeldt, R. Knitter, Long-term thermal stability of two-phased lithium orthosilicate/metatitanate ceramics, J. Nucl. Mater. 507 (2018) 396–402, https://doi.org/10.1016/j.jnucmat.2018.05.010.
[19] A. Antuzevics, A. Zarins, A. Ansone, J. Cipa, G. Kizane, J.M. Leys, R. Knitter, Thermal properties of paramagnetic radiation-induced defects in lithium orthosilicate containing breeder material, J. Nucl. Mater. 565 (2022) 153713, https://doi.org/10.1016/j.jnucmat.2022.153713.
[20] A. Zarins, A. Antuzevics, G. Kizane, J.M. Leys, R. Knitter, Simulations of complex electron paramagnetic resonance spectra for radiation-induced defect centres in advanced ceramic breeder pebbles, Nucl. Mater. Energy 35 (2023) 101458, https://doi.org/10.1016/j.nme.2023.101458.
[21] A. Antuzevics, A. Zarins, J. Cirulis, A. Fedotovs, A. Ansone, M. Rzepna, J.M. Leys, R. Knitter, Hyperfine interactions of paramagnetic radiation-induced defect centres in advanced ceramic breeder pebbles, Nucl. Mater. Energy 40 (2024) 101698, https://doi.org/10.1016/j.nme.2024.101698.
[22] B. Konar, M.-A. Van Ende, I.-H. Jung, Critical evaluation and thermodynamic optimization of the Li-O, and Li_2O-SiO_2 systems, J. Eur. Ceram. Soc. 37 (2017) 2189–2207, https://doi.org/10.1016/j.jeurceramsoc.2016.12.041.
[23] R. Knitter, B. Alm, G. Roth, Crystallisation and microstructure of lithium orthosilicate pebbles, J. Nucl. Mater. 367–370 (2007) 1387–1392, https://doi.org/10.1016/J.JNUCMAT.2007.04.002.
[24] H. Kleykamp, Enthalpy, heat capacity, second-order transitions and enthalpy of fusion of Li_4SiO_4 by high-temperature calorimetry, Thermochim Acta 287 (1996) 191–201, https://doi.org/10.1016/S0040-6031(96)02996-6.
[25] T. Tokunaga, T. Matsui, Y. Arita, H. Yokoi, Phase transitions of Li_2ZrO_3 and Li_4SiO_4 at high temperatures by DTA and EXAFS analysis, High Temperatures – High Pressures 28 (1996) 629–636.
[26] C. Masquelier, H. Kageyama, T. Takeuchi, Y. Saito, O. Nakamura, Chemistry and structure analysis in the $Li_{1+x}B_xSi_{1-x}O_4$ solid solution, J. Power Sources 54 (1995) 448–451, https://doi.org/10.1016/0378-7753(94)02122-J.
[27] M. Asou, T. Terai, Y. Takahashi, High-temperature enthalpy-increment measurements and derived heat capacity of lithium orthosilicate (Li_4SiO_4) at temperatures from 300 K to 1000 K, J. Chem.Thermodyn. 24 (1992) 273–280, https://doi.org/10.1016/S0021-9614(05)80067-9.
[28] R. Brandt, B. Schulz, Specific heat of some Li-compounds, J. Nucl. Mater. 152 (1988) 178–181, https://doi.org/10.1016/0022-3115(88)90324-8.
[29] G.W. Hollenberg, A transformation in lithium orthosilicate, J. Nucl. Mater. 103 (1981) 591–596, https://doi.org/10.1016/0022-3115(82)90663-8.
[30] A.R. West, F.P. Glasser, Crystallisation of lithium zinc silicates, Part 1 phase equilibria in the system Li_4SiO_4-Zn_2SiO_4, J. Mater. Sci. 5 (1970) 557–565, https://doi.org/10.1007/BF00554364.
[31] A.R. West, F.P. Glasser, Crystallisation of lithium zinc silicates, Part 2 comparison of the metastable and stable phase relations and the properties of the lithium zinc orthosilicates, J. Mater. Sci. 5 (1970) 676–688, https://doi.org/10.1007/BF00549752.
[32] D.A.H. Hanaor, M.H.H. Kolb, Y. Gan, M. Kamlah, R. Knitter, Solution based synthesis of mixed-phase materials in the Li_2TiO_3–Li_4SiO_4 system, J. Nucl. Mater. 456 (2015) 151–161, https://doi.org/10.1016/j.jnucmat.2014.09.028.
[33] H. Kleykamp, Phase equilibria in the Li–Ti–O system and physical properties of Li_2TiO_3, Fusion Eng. Des. 61–62 (2002) 361–366, https://doi.org/10.1016/S0920-3796(02)00120-5.
[34] A. Zarins, A. Ansone, M. Senko, J. Cipa, A. Antuzevics, L. Avotina, L. Baumane, G. Kizane, M. Gonzalez, J.M. Leys, R. Knitter. Influence of various radiation types on radiation-induced processes in lithium orthosilicate-based ceramic breeder materials. Proceedings of 21st International Workshop on the Ceramic Breeder Blanket Interactions (CBBI-21), 19-20 October 2023, Granada, Spain, p. 576-591. https://info.fusion.ciemat.es/media/CBBI-21_Proceedings_2023.pdf.
[35] J. Ortiz-Landeros, L. Martinez-dlCruz, C. Gomez-Yanez, H. Pfeiffer, Towards understanding the thermoanalysis of water sorption on lithium orthosilicate (Li_4SiO_4), Thermochim Acta 515 (2011) 73–78, https://doi.org/10.1016/j.tca.2010.12.025.
[36] A. Zarins, O. Valtenbergs, G. Kizane, A. Supe, S. Tamulevicius, M. Andrulevicius, E. Pajuste, L. Baumane, O. Leys, M.H.H. Kolb, R. Knitter, Characterisation and radiolysis of modified lithium orthosilicate pebbles with noble metal impurities, Fusion Eng. Des. 124 (2017) 934–939, https://doi.org/10.1016/j.fusengdes.2017.01.008.
[37] T. Nakazawa, D. Yamaki, K. Noda, A study on irradiation-induced structural change of lithium orthosilicate by infrared spectroscopy analysis with MNDO calculation, J. Nucl. Mater. 248 (1997) 121–127, https://doi.org/10.1016/S0022-3115(97)00168-2.
[38] E. Carella, T. Hernandez, The effect of γ-radiation in Li_4SiO_4 ceramic breeder blankets, Fusion Eng. Des. 90 (2015) 73–78, https://doi.org/10.1016/j.fusengdes.2014.11.010.
[39] Q. Zhou, Y. Mou, X. Ma, L. Xue, Y. Yan, Effect of fuel-to-oxidizer ratios on combustion mode and microstructure of Li_2TiO_3 nanoscale powders, J. Eur. Ceram. Soc. 34 (2014) 801–807, https://doi.org/10.1016/j.jeurceramsoc.2013.10.004.
[40] E.M. Masoud, S. Indris, Block-shaped pure and doped $Li_4Ti_5O_{12}$ containing a high content of a Li_2TiO_3 dual phase: an anode with excellent cycle life for high rate performance lithium-ion batteries, RSC Adv. 5 (2015) 108058–108066, https://doi.org/10.1039/C5RA22745C.
[41] M.H. Brooker, J.B. Bates, Raman and infrared spectral studies of anhydrous Li_2CO_3 and Na_2CO_3, J. Chem. Phys. 54 (1971) 4788–4796, https://doi.org/10.1063/1.1674754.
[42] X. Wang, W. Xia, X. Sun, Y. Yang, X. Ren, Y. Li, Hydrothermal-calcination synthesis of lithium orthosilicate microspheres for high-temperature CO_2 capture, Carbon Capture Sci. Technol. 13 (2024) 100303, https://doi.org/10.1016/j.ccst.2024.100303.
[43] O. Leys, C. Odemer, U. Maciejewski, M.H.H. Kolb, R. Knitter, Microstructure analysis of melt-based lithium orthosilicate/metatitanate pebbles, Practical Metallography 50 (2013) 196–204, https://doi.org/10.3139/147.110194.
[44] G.M.L. Piccolo, M. Cannas, S. Agnello, Intrinsic point defects in silica for fiber optics applications, Materials 14 (2021) 7682, https://doi.org/10.3390/ma14247682.
[45] D.L. Griscom, Defect structure of glasses: some outstanding questions in regard to vitreous silica, J. Non Cryst. Solids 73 (1985) 51–77, https://doi.org/10.1016/0022-3093(85)90337-0.